Structure, Vol. 11, 973–984, August, 2003, ©2003 Elsevier Science Ltd. All rights reserved. DOI 10.1016/S0969-2126(03)00151-5

The Structure of Barley α-Amylase Isozyme 1 Reveals a Novel Role of Domain C in Substrate Recognition and Binding: A Pair of Sugar Tongs

Xavier Robert,[1] Richard Haser,[1,*] Tine E. Gottschalk,[2] Fabien Ratajczak,[3] Hugues Driguez,[3] Birte Svensson,[2] and Nushin Aghajari[1]

[1]Laboratoire de BioCristallographie
Institut de Biologie et Chimie des Protéines
UMR 5086-CNRS/UCBL1
7 Passage du Vercors
F-69367 Lyon cedex 07
France

[2]Department of Chemistry
Carlsberg Laboratory
Gamle Carlsberg Vej 10
DK-2500 Copenhagen Valby
Denmark

[3]Centre de Recherche sur les Macromolécules Végétales
CNRS (affiliated with Université Joseph Fourier)
BP 53
F-38041 Grenoble
France

Summary

Though the three-dimensional structures of barley α-amylase isozymes AMY1 and AMY2 are very similar, they differ remarkably from each other in their affinity for Ca^{2+} and when interacting with substrate analogs. A surface site recognizing maltooligosaccharides, not earlier reported for other α-amylases and probably associated with the different activity of AMY1 and AMY2 toward starch granules, has been identified. It is located in the C-terminal part of the enzyme and, thus, highlights a potential role of domain C. In order to scrutinize the possible biological significance of this domain in α-amylases, a thorough comparison of their three-dimensional structures was conducted. An additional role for an earlier-identified starch granule binding surface site is proposed, and a new calcium ion is reported.

Introduction

α-amylases (1,4-α-D-glucan glucanohydrolase; EC 3.2.1.1) are monomeric enzymes widely occurring in animals, plants, and microorganisms. They catalyse the hydrolysis of internal α-D-(1,4)-glucosidic linkages in starch (amylose and amylopectin), glycogen, and related oligo- and polysaccharides to produce maltodextrins, maltooligosaccharides, and glucose. Seed germination is triggered by an increase in temperature and humidity and causes the embryo to synthesize the phytohormone gibberellic acid, which induces de novo synthesis of α-amylase and an array of other hydrolases (Jones and Jacobsen, 1991). The progressive release of sugars from the storage starch provides energy to the growing plantlet.

In germinating barley seeds, different α-amylase isozymes, encoded by two multigene families and referred to as AMY1 and AMY2, are distinguished (Jones and Jacobsen, 1991; Rogers, 1985b; Rogers and Milliman, 1983). Whereas the two isozymes, which contain 414 and 403 amino acid residues, respectively, display 80% sequence identity, they are very distantly related to α-amylases from microorganisms and animals (Rogers, 1985a). Indeed α-amylases from different sources have only nine identical residues (MacGregor et al., 2001). Despite the high sequence identity, AMY1 and AMY2 show distinctly different physicochemical and biochemical properties. AMY1 is known as the low-pI (pI = 4.9) isozyme, and AMY2 is known as the high-pI (pI = 5.9) isozyme (Jones and Jacobsen, 1991). AMY1 has highest affinity for calcium ions (Bertoft et al., 1984; Bush et al., 1989; Rodenburg et al., 1994), is the most stable at acidic pH (Rodenburg et al., 1994), and is the least stable at elevated temperature (Bertoft et al., 1984). Moreover, AMY1 has the highest affinity and activity toward starch granules (MacGregor and Ballance, 1980; MacGregor and Morgan, 1986; Søgaard and Svensson, 1990), whereas, on soluble substrates (Ajandouz et al., 1992; MacGregor et al., 1994; Søgaard and Svensson, 1990), AMY1 still has the highest affinity, but AMY2 has the highest turnover rate. Finally, a most remarkable difference is the unique capacity of AMY2 in binding the endogenous bifunctional inhibitor BASI (barley α-amylase/subtilisin inhibitor) (Abe et al., 1993; Leah and Mundy, 1989; Mundy et al., 1983; Sidenius et al., 1995; Svendsen et al., 1986).

It has been shown earlier, by UV difference spectroscopy, differential labeling, site-directed mutagenesis, and crystallography (Gibson and Svensson, 1987; Kadziola et al., 1998; Søgaard et al., 1993), that AMY1 contains a separate surface binding area on the basis of two contiguous tryptophans, Trp278 and 279 (Trp276 and 277 in AMY2). This site has low affinity for acarbose (K_d = 5 mM) and binds β-cyclodextrin in competition with starch granules, and the Trp279Ala mutant has ten- and three-fold-reduced affinity for starch granules and β-cyclodextrin, respectively (Søgaard et al., 1993). No mutant was obtained at Trp278, which is invariant in cereal α-amylases (Søgaard et al., 1993). Sequence comparison suggests that this starch binding site is unique to α-amylases from higher plants, whereas other surface binding sites are reported in certain microbial or mammalian enzymes (Brzozowski et al., 2000; Larson et al., 1994; Qian et al., 1995).

Here we report the first crystal structures of native AMY1 and AMY1 in complex with the substrate analog, methyl $4^{I},4^{II},4^{III}$-trithiomaltotetraoside, henceforth referred to as thio-DP4. These structures are compared to those of native AMY2 and AMY2 in complex with the pseudotetrasaccharide inhibitor acarbose (Kadziola et al., 1994, 1998), which is a well known transition-state analog for α-amylases and numerous other α-glucoside hydrolases and transferases (Truscheit et al., 1981). The

*Correspondence: r.haser@ibcp.fr

structural analysis carried out here will focus on calcium ion and oligosaccharide binding.

Results and Discussion

Overall Structure

Barley α-amylase 1 (AMY1) displays the overall form of an ellipsoid, with dimensions of approximately 68 Å × 53 Å × 36 Å. The three-dimensional truncated structure consisting of 404 amino acid residues is very similar to that of AMY2 (Kadziola et al., 1994) (rmsd for main chain atoms is 0.63 Å) and has all side chains clearly defined. A few loops differ slightly in spatial localization (Robert et al., 2002b). Because of the high-resolution data, sixteen residues displaying double conformations have been identified. Among these, Met53, Arg183, and Met298 have been reported as being important in substrate binding at the active site cleft (André et al., 1999; Kadziola et al., 1998; Matsui and Svensson, 1997; Mori et al., 2001, 2002). A truncated form (AMY1Δ9) in which residues 406–414 were eliminated to obtain a C terminus matching that of AMY2 was used for crystallization and structure determination (Robert et al., 2002a). As severe difficulties in crystallizing both wild-type (Svensson et al., 1987) and recombinant full-length AMY1 (Robert et al., 2002a) were overcome with AMY1Δ9, the C-terminal segment in AMY1 appears to be very flexible or highly disordered. The C-terminal Asn405 in AMY1Δ9 was not included in the structure because of lacking $2F_o - F_c$ and $F_o - F_c$ electron density.

In the refined 1.5 Å resolution AMY1 structure, nine molecules of ethylene glycol (used as cryoprotectant) and 809 water molecules are present. Finally, the crystal structure of full-length AMY1 has also been solved, but its refinement was not completed because of medium quality data to 2.5 Å resolution (Robert et al., 2002a). The three-dimensional structure of full-length AMY1 is the same as that of AMY1Δ9, with the exception of a few residues that were not defined in the electron density map, as reflected by the rmsd on main chain atoms of 0.53 Å. Hereafter, we only deal with the recombinant truncated form, which will be referred to as AMY1.

AMY1, as do the vast majority of known α-amylase structures, contains three domains, including a major central domain with a parallel $(\beta/\alpha)_8$ barrel super-secondary structure (domain A) (Robert et al., 2002b). As in AMY2, domain A differs from the classical TIM barrel (Banner et al., 1975), by having three additional α helices, A-α_{6a}, A-α_{7a}, and A-α_{8a}, extending from β strands A-β_6, A-β_7, and A-β_8, respectively (Figure 1). An irregular loop of 65 residues (domain B) bulges from the $(\beta/\alpha)_8$ barrel between β_3 and α_3 and forms an antiparallel twisted β sheet with the protruding domain A loop A-$\beta_2\alpha_2$, which is considered as an integral part of domain B. Although AMY1 has a higher affinity for calcium ions than does AMY2 (Bush et al., 1989), domain B in both isozymes binds three Ca^{2+} ions (Ca500, Ca501, and Ca502), which have been proposed to be critical for folding and conformational stability and, hence, for the enzyme activity (Bertoft et al., 1984; Bush et al., 1989). The overlay of AMY1 and AMY2 structures shows that the only difference between these three Ca^{2+} binding sites is the presence of an additional water molecule (Wat788) as a ligand for Ca502 in AMY1 (Robert et al., 2002b). This may very well be explained by the lower-resolution data of AMY2, since a water molecule with low occupancy was reported, but not included in the three-dimensional structure of AMY2 (Kadziola et al., 1994). Finally, the 61-residue-long C-terminal domain (domain C) is organized as a five-stranded antiparallel β sheet. The connection between β strands C-β_3 and C-β_4 is ensured by a long transverse loop protruding from the plane of the β sheet as in AMY2. Hereof results a topology where β strands C-β_1, C-β_3, and C-β_4 are parallel and run antiparallel to C-β_2 and C-β_5. The overall 3D structure of the AMY1/thio-DP4 complex is highly similar to that of the free enzyme but contains an extra Ca^{2+} ion located in the active site, as described later.

Analysis of the Catalytic Site Reveals a Fourth Ca^{2+} Ion in AMY1/Thio-DP4

The three catalytic residues in AMY1, Asp180, Glu205, and Asp291, are perfectly superimposable with their homologs in AMY2 (Figures 2A and 2B). Analysis of the active site was focused on residues for which counterparts bind acarbose in the complex with AMY2 (Kadziola et al., 1998): Tyr51, His92, Arg177, Asp179 (catalytic), Lys182, Glu204 (catalytic), Trp206, Ser208, His288, and Asp289 (catalytic). These residues are conserved in AMY1, with the exception of $Lys182_{AMY2}$ and $Ser208_{AMY2}$ being replaced by $Arg183_{AMY1}$ and $Asn209_{AMY1}$, respectively. In AMY1 the side chains of Arg183 and Asn209 are oriented in the same direction, while the corresponding AMY2 side chains, Lys182 and Ser208, point in opposite directions (Figure 2B). A total of 15 hydrogen bond contacts were established between enzyme and the inhibitor in the active site cleft of AMY2/acarbose (Kadziola et al., 1998). Whereas only water molecules are present in the catalytic site in native AMY1, examination of the electron density in the active site of the AMY1/thio-DP4 complex surprisingly revealed no trace of the thio-DP4 sugar but did reveal a Ca^{2+} ion (Ca503). This Ca^{2+} site has been confirmed in AMY1/thio-DP4 by an anomalous difference Patterson map, which clearly showed peaks for Ca500, Ca501, and Ca502 as a good internal reference. The lack of sugar binding is in agreement with thio-DP4 showing no inhibition of the AMY1-catalyzed hydrolysis (M.T. Jensen and B.S., unpublished data). It is worth mentioning that Ca503, though it is not directly superimposable, is located at the level of the interglycosidic nitrogen in the complex AMY2/acarbose (Kadziola et al., 1998), i.e., between subsites −1 and +1 (Figure 2B). Furthermore, it is at exactly the same position as the fully hydrated Ca^{2+} ion present at the protein interface in AMY2/BASI (Vallée et al., 1998). One distinct difference between Ca503 and its counterpart in AMY2/BASI is the spatial organization of the surrounding water molecules. In AMY1/thio-DP4, the five water molecules are organized as a regular pentagon, with Ca503 at the center (Figure 2A). The sixth water molecule is located above Ca503, the ensemble thus defining a pyramid with a pentagonal base. This difference in the organization of water molecules in the two structures may be due to the water molecules being forced to adopt another ar-

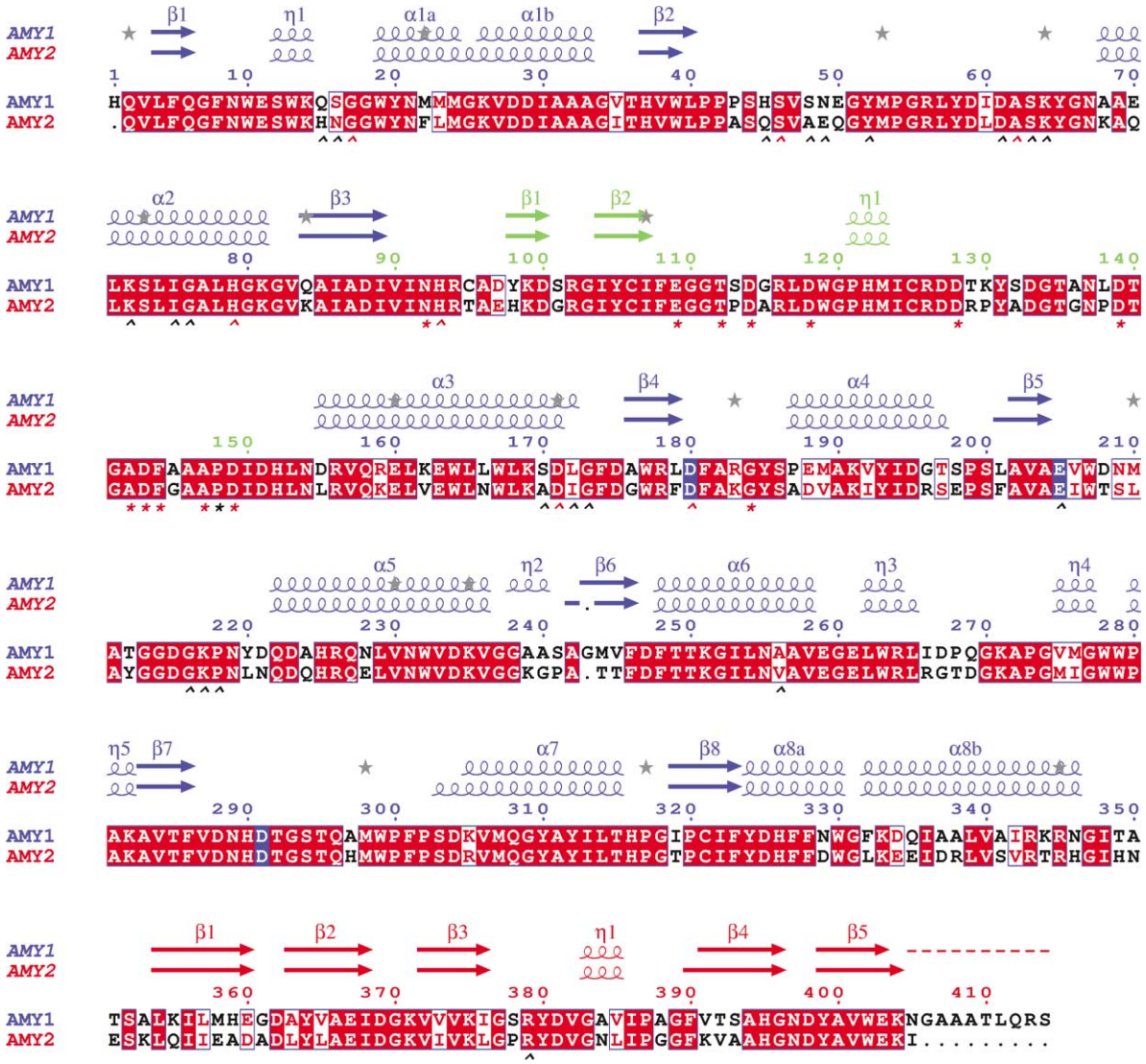

Figure 1. Sequence Alignment of AMY1 and AMY2

Secondary structures of the two isozymes are indicated above the alignment and colored as a function of domains: domain A, blue; domain B, green; domain C, red. β strands, arrows; α helices, helices. Catalytic residues are highlighted in blue. Residues in double conformation in the 3D structure of AMY1, gray stars. Ligands to calcium ions are indicated below the sequence by an asterisk, whereas ligands to ethylene glycol molecules in the native structure are indicated with the caret (^) symbol. For both types of ligand, distances shorter than 3.2 Å are indicated in red, and distances between 3.2 and 4.0 Å are indicated in black.

rangement in the absence of BASI, to fill the space around Ca503 and maximize the contact with the neighboring amino acid side chains. Surprisingly, no electron density corresponding to a Ca^{2+} ion was observed in the native AMY1 structure, and the water molecules were organized quite differently than those in the AMY1/thio-DP4 complex. At present, Ca503 in this complex cannot be explained by a local structure rearrangement compared to the native AMY1 structure or by a difference in crystallization conditions. It should be mentioned that the AMY1 stock solution contains 100 mM $CaCl_2$, leading to a concentration of 40 mM in the drop (Robert et al., 2002a), which was higher than the $CaCl_2$ concentration in the thio-DP4 soaking experiment. Thus, whether this active site calcium has a role of a modulator or is related to a local pH variation remains to be clarified. Ca^{2+} was demonstrated to exert an isozyme-specific effect on the activity of AMY1 and AMY2 toward starch (Rodenburg et al., 1994, 2000; Juge et al., 1995). While AMY1 has the highest affinity for Ca^{2+} of the two isozymes (Bush et al., 1989), it also shows variation in activity, the maximum activity being in the range of 0.02–1.0 mM $CaCl_2$. AMY2, in contrast, has highest activity at 10–15 mM $CaCl_2$. At these higher concentrations the activity of AMY1 declines, and, eventually, at 50 mM, very low residual activity is shown for both isozymes.

The AMY1 structure contains a water-filled pocket formed by a chain of water molecules (Wat603, Wat605, Wat625, Wat755, Wat626, and Wat607), running from the active site toward the interior of the protein. Com-

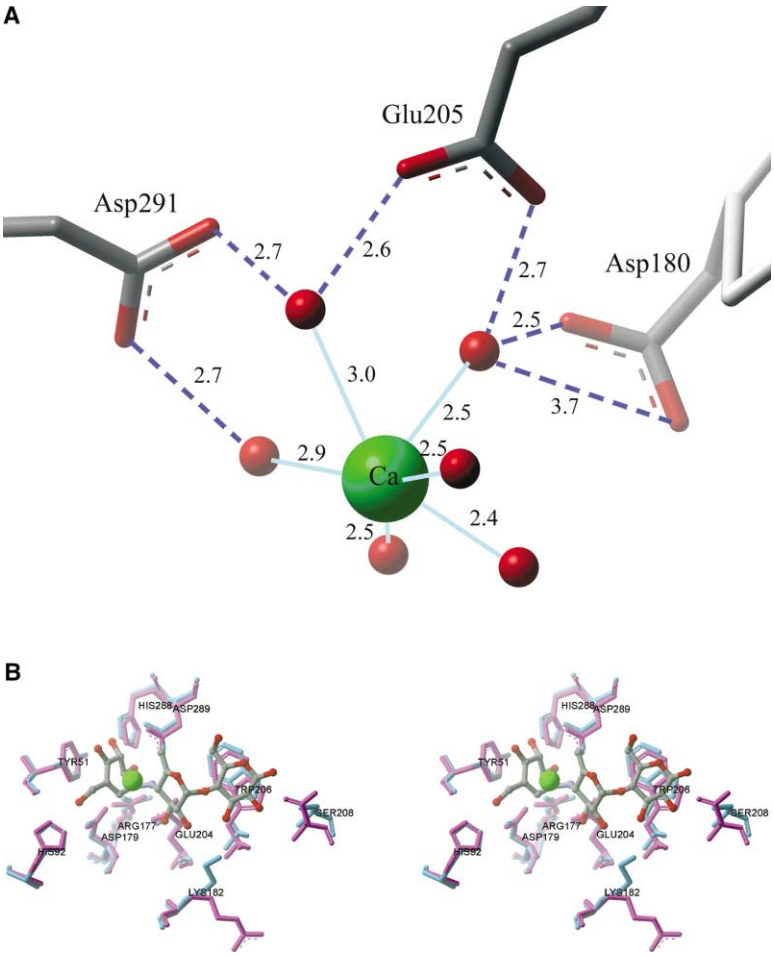

Figure 2. Active Site Views

(A) Interactions between Ca503 and the catalytic residues in AMY1. Calcium ion, green sphere; water molecules, red spheres; hydrogen bonds, dashed blue lines; coordination bonds, plain cyan lines. Distances are in angstroms.

(B) Superimposition of active sites of the AMY1/thio-DP4 and AMY2/acarbose complexes. AMY1, purple; AMY2, blue. The acarbose fragment bound to AMY2 is shown in ball and stick with standard color-coding. Ca503, green sphere. Labels correspond to AMY2 numbering.

pared to AMY2, which also displays this water pocket (Kadziola et al., 1998), an additional water molecule (Wat 755) was located. In AMY2 as well as in the AMY2/acarbose complex, Wat607, which bridges the carboxylate groups of two catalytic residues, Glu204 and Asp289, was proposed as a good candidate for being the so-called "catalytic" water molecule in the hydrolytic reaction (Kadziola et al., 1998). A similar pocket was observed in *Ps. haloplanctis* α-amylase (Aghajari et al., 1998b).

The Starch Granule Binding Surface Site

In the structure of AMY1/thio-DP4, two rings from the tetrasaccharide stack onto a pair of consecutive tryptophans, Trp278 and Trp279 (Figure 3), also known as the starch granule binding surface site (Gibson and Svensson, 1987; Kadziola et al., 1994, 1998; Søgaard et al., 1993). Substitution of the interglycosidic oxygen atoms by sulphur in thio-DP4 (Figure 4A) renders this sugar noncleavable by α-amylases. The fact that only electron density corresponding to two of four rings is observed at this site may be a consequence of a disordered arrangement of the two remaining sugar rings. Indeed, this surface site is highly exposed to the solvent, and no symmetry-related molecule is present to stabilize the bound thio-DP4 sugar. Though the electron density is rather poor around the sugar rings, it clearly reveals the presence of the interglycosidic sulphur atom. Besides the hydrophobic stacking to the indole rings of Trp278 and Trp279, the two rings of thio-DP4 form six hydrogen bonds to Trp278 and neighboring residues in the structure (Gln227 and Asp234). A disaccharide unit also stacks onto these tryptophans (Trp276 and Trp277 in AMY2) with five hydrogen bond interactions in the structure of AMY2/acarbose (Kadziola et al., 1998), but, even though the latter complex is solved at 2.8 Å, versus 2.0 Å for AMY1/thio-DP4, the electron density for the disaccharide unit in the structure of AMY2/acarbose is better defined than that for the disaccharide in the thio-DP4 complex structure. The differences in electron density quality for the ligand molecules in these two complexes may be explained by the variation in geometries of substrate analogs, in particular, the angle between the two successive sugar rings. This angle, defined by C1 of ring A in acarviosine (see Figure 4B), the interglycosidic nitrogen atom between units A and B, and C4 in ring B, is 125°. The corresponding angle in the bound thio-DP4 is smaller and close to 100° because of the interglycosidic sulphur, while, in natural substrates, this angle approximates 115°. The angle between the planes formed by the two indole rings in Trp278 and Trp279 is around 135° and highly constant between AMY1 and AMY2 in both native and complexed structures. In AMY2/acarbose the angle between the two sugar moieties is thus better adapted to this stacking interaction

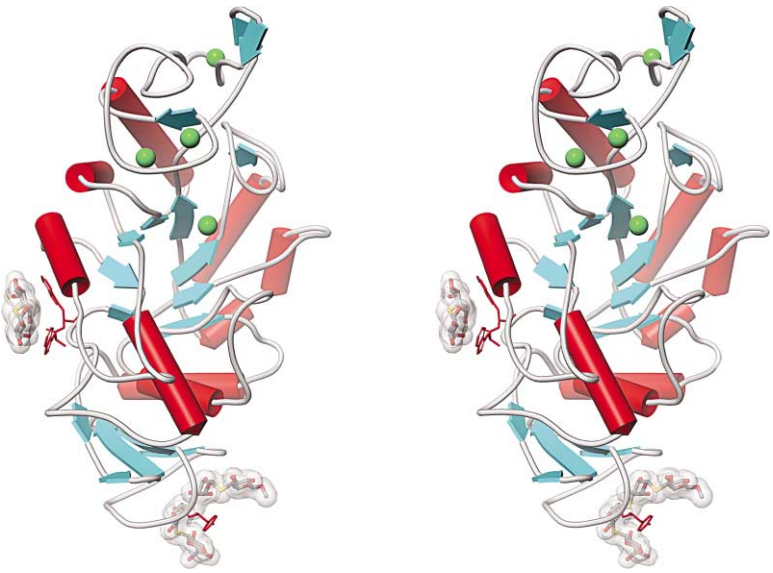

Figure 3. Overall Structure of AMY1 in Complex with Thio-DP4

Calcium ions, green spheres. The three upper calcium ions are those found both in AMY1 and AMY2 (Ca500, Ca501, and Ca502). The fourth Ca503 is located close to the center of the $(\beta/\alpha)_8$ barrel, where it occupies the active site (see Figures 2A and 2B). Thio-DP4 substrate analog fragments are shown as surface representations. To the left, the starch granule binding surface site on domain A is shown with the two tryptophan residues (Trp278 and Trp279) highlighted in red. In domain C (bottom part of the figure), an entire thio-DP4 molecule is curved around Tyr380 at the level of the sugar tongs.

than the smaller angle of 100° in thio-DP4. The closer the planes determined by the two indole rings and the plane of the sugar rings (in chair form) are to being ideally parallel, the stronger the forces in the hydrophobic stacking (Quiocho, 1989). It seems that the ideal angle of the glycoside bond for this interaction is between 120° and 135°.

This surface binding site seems to possess the special capacity of selecting substrates, according to their geometrical characteristics, probably governed by the surroundings of this site. Indeed, the two tryptophans adopt a locked conformation because of a very tight packing with neighboring residues (Arg226, Gln227, Val230, Asp234, Pro280, and Lys282). Owing to this environment, the side chains of Trp278 and Trp279 are restrained in their orientations. We propose that this ensemble constitutes a "geometric filter" that favors binding of structurally complementary molecules. If this hypothesis is correct, it may explain why thio-DP4 is lacking in the active site.

A Tyrosine Essential for a New Sugar Binding Site in Domain C: The "Sugar Tongs"

In the AMY1/thio-DP4 complex, electron density corresponding to an entire molecule of thio-DP4 was observed in the vicinity of Tyr380 in domain C. In contrast to the surface binding site described above, the electron density at this second surface site was well defined and continuous, including all four sugar rings and leaving doubt about neither the orientation of this tetrasaccharide nor the nature of its atoms. As seen in Figure 4C, nine direct hydrogen bonds are formed between sugar rings and AMY1 residues Lys375, Tyr380, Asp381, Val382, His395, and Asp398, where Val382 and Asp398 interact with oxygen atoms of thio-DP4 via their peptide nitrogen. Moreover, the carbonyl oxygen in Tyr380 makes direct hydrogen bonds to two hydroxyl groups from the sugar and several hydrophobic contacts to Thr392, Tyr399, and Trp402, whereas the phenol ring makes five hydrophobic contacts to the two sulphur atoms of the trisaccharide unit at the reducing end (Figure 4C). Finally, the glucose unit at the nonreducing end extends into the solvent and makes one hydrogen bond to the protein (Asp398) and two hydrophobic contacts with Tyr380. This explains the high average B factor for this ring (57.9 Å^2) as compared to those of the three others (32.0 Å^2, 14.4 Å^2, and 24.6 Å^2) being stabilized through a higher number of interactions with the protein. Remarkably, all these interacting amino acid residues exist in AMY2, with the exception of $Thr392_{AMY1}$, which is a valine in AMY2, but this does not seem to be determinant for why only AMY1 binds maltooligosaccharides to domain C.

Of these residues Tyr380 clearly has a key role in the binding of thio-DP4 to domain C, since, out of a total of 17 contacts to the ligand, this residue makes 8 (5 hydrophobic contacts and 3 hydrogen bonds). The critical role of $Tyr380_{AMY1}$ is emphasized by the superimposition of the structures of native AMY1 on AMY1/thio-DP4, showing that Tyr380 has moved in the complex to entrap the sugar (Figure 5). The comparison of the two structures shows that the C_α and the phenol oxygen of $Tyr380_{AMY1}$ shift 1.2 and 3.1 Å, respectively. The short loop preceding Tyr380 is flexible in AMY1, whereas it seems more restrained in AMY2, with Pro376 (Ser378 in AMY1) only two positions from $Tyr378_{AMY2}$. The residue at this position ($Ser378_{AMY1}$/$Pro376_{AMY2}$) is thus proposed to be a major determinant of an isozyme-specific difference in the flexibility of this loop, which may control maltooligosaccharide binding to domain C.

Other clear differences are found between the two isozymes in domain C. One of the most remarkable is a large negatively charged surface area in AMY1 close to Tyr380, which stems from Asp381 (see Figure 5C). In AMY2 the side chain of the corresponding $Asp379_{AMY2}$ is orientated away from $Tyr378_{AMY2}$, while, in AMY1, Asp381 has the same orientation as $Tyr380_{AMY1}$. Subtle differences in the backbone conformation and, particularly, in the peptide bonds from $Asp381_{AMY1}$, $Val382_{AMY1}$, and $Gly383_{AMY1}$ seem to cause these differences in orienta-

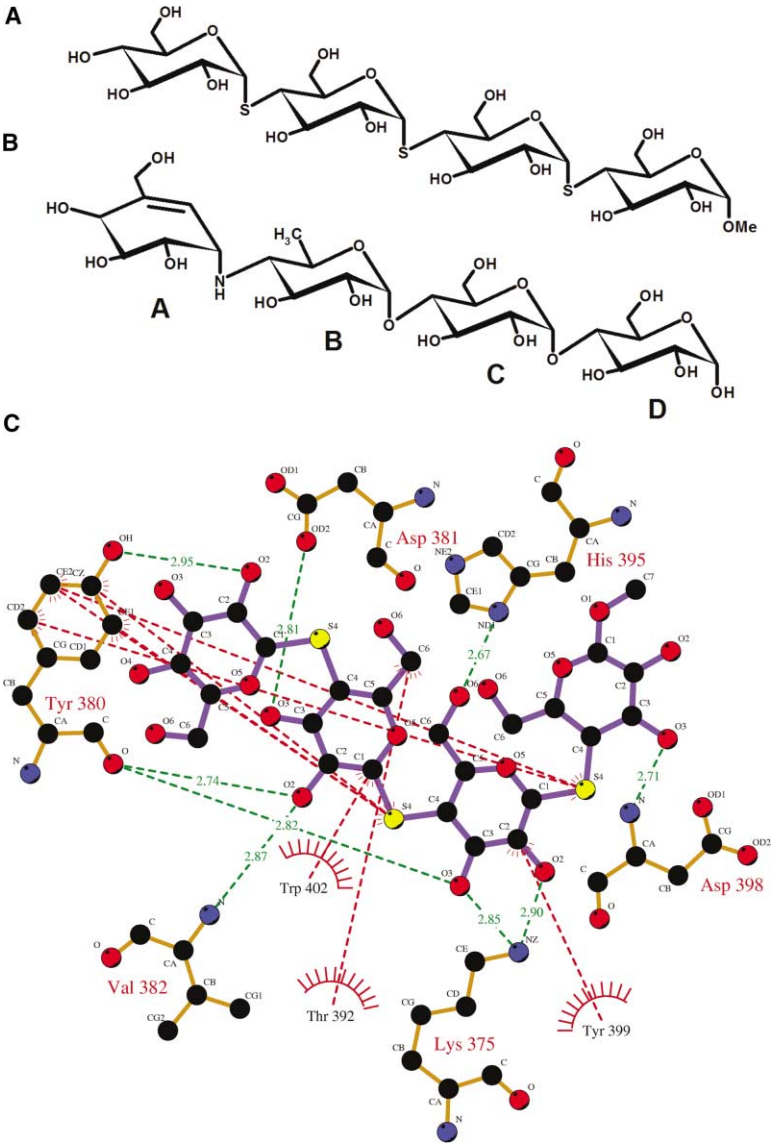

Figure 4. Substrate Analogs

(A) Chemical structure of the thio-DP4 substrate analog.

(B) Chemical structure of acarbose. Rings are labeled as referred to in the text. Rings A and B constitute the acarviosine unit, which is α-1,4 linked to a maltose unit (rings C and D).

(C) Schematic representation of interactions in the domain C sugar tongs site, between AMY1 and thio-DP4. The substrate analog is shown in ball and stick in purple. AMY1 ligand side chains, orange. Carbon atoms, black; oxygen, red; nitrogen, blue; sulphur, yellow. Direct hydrogen bonds between the protein and thio-DP4, dashed green lines (lengths in Å); hydrophobic contacts, dashed red lines. This figure was generated with the program Ligplot (Wallace et al., 1995).

tion. Noticeably, Asp381-Oδ2 in AMY1/thio-DP4 is hydrogen bonded to thio-DP4 (Figure 4C).

Structure Comparison of C Domains from Different α-Amylases

To further analyze the implication of domain C in maltooligosaccharide binding, we compared the structures of C domains in AMY1, AMY2, and ten α-amylases from different species. Domain C in α-amylase structures solved to date is mostly composed of antiparallel β strands, and $Tyr380_{AMY1}$ is only present in AMY2 (Tyr378) (Figure 6). Furthermore, among the set of compared structures, AMY1 and AMY2 have the smallest domain C, with five β strands, whereas those in α-amylases from *B. licheniformis* and *B. stearothermophilus* have seven β strands, and those from *A. niger*, *A. oryzae, Ps. Haloplanctis*, and *B. subtilis* have eight β strands. Finally, insect (*T. molitor*) and mammalian α-amylases (human salivary, human pancreas, and porcine pancreas) have ten β strands (Figure 6). The smaller structural organization seems to be one of the major determinants of the ability of domain C in AMY1 to bind sugar molecules.

These studies show that α-amylases from *B. licheniformis* and *B. stearothermophilus* in general display very different spatial organization, despite the apparent secondary structure conservation in the alignment, and it is impossible to superimpose the secondary structure elements succeeding β1 with those in the ten other α-amylases (Figure 6, indicated by the β strands in black). For the ten remaining structures, the major difference is that β4 in AMY1 and AMY2 is not entirely superimposed with β strands in the other enzymes, since, spatially speaking, this one β strand in AMY1 and AMY2 corresponds to two separate β strands in the other α-amylases (Figure 6).

Careful examination of the topologies shows that the eight α-amylases that are comparable to AMY1 and AMY2 contain either two or three additional β strands, all inserted between β4 and β5. These eight enzymes, however, share two well-superimposed β strands (Figure 6, purple and dark green). This motif thus character-

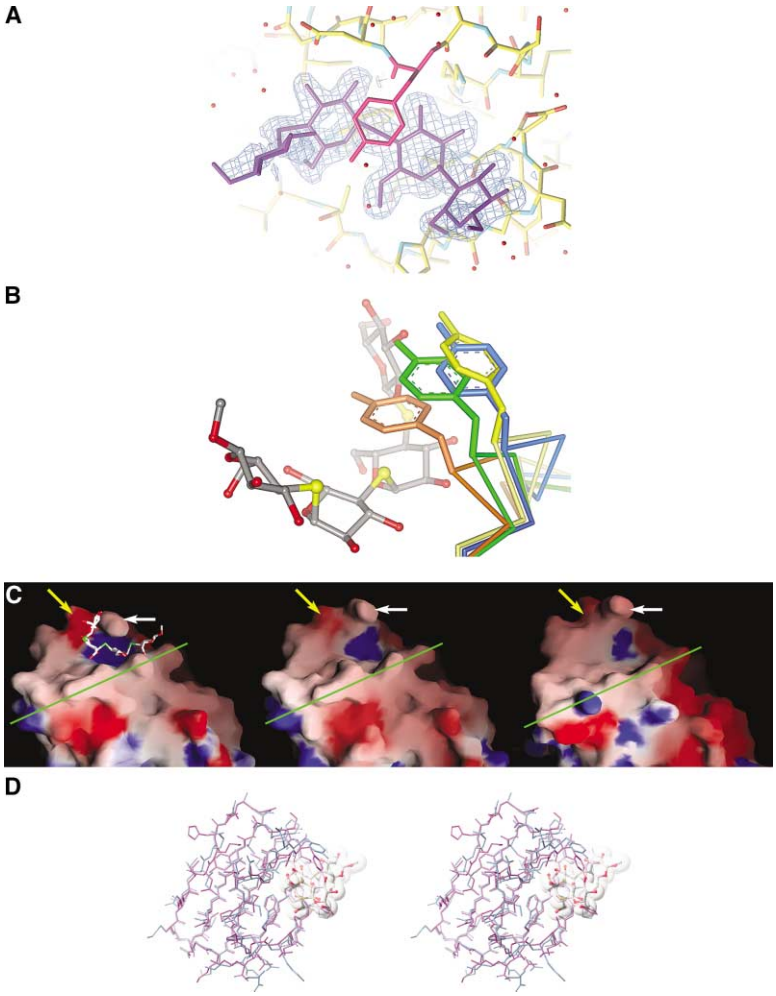

Figure 5. Close-up of the Sugar Tongs

(A) Close-up of the sugar tongs in AMY1. The electron density ($2F_o - F_c$ map contoured at 1 σ) is only shown for the thio-DP4 substrate analog (purple). The methylated hydroxy group at the reducing end is seen to the right. All four sugar rings of the substrate analog are present in the electron density. Tyr380 involved in binding, pink.

(B) Close-up of the sugar tongs and $Tyr380_{AMY1}$/$Tyr378_{AMY2}$ side chain positions in native states or in complex with substrate analogs. Tyrosine in yellow corresponds to the native AMY2 structure, in blue to AMY2/acarbose, in green to native AMY1, and in orange to AMY1 in complex with the thio-DP4 substrate analog, which is shown in ball and stick representation with standard color-coding.

(C) Comparison of the domain C surface of, from left to right, AMY1/thio-DP4, native AMY1, and AMY2 colored as a function of charges. $Tyr380_{AMY1}$/$Tyr378_{AMY2}$, white arrow; the plane defined by the five antiparallel β strands, green line (see also Figure 7). $Asp381_{AMY1}$/$Asp379_{AMY2}$, yellow arrow. Negative charges, red; positive charges, blue. Representations are generated with the program GRASP (Nicholls et al., 1991) and are on the same scale.

(D) Superimposition of the C domain of AMY1/thio-DP4 on that of AMY2. AMY1/thio-DP4, purple; AMY2, blue. Thio-DP4 is shown in ball and stick presentation with standard color-coding.

izes the category of α-amylases with eight β strands in domain C. α-Amylases from human saliva, human and porcine pancreas, and *T. molitor* further display two very short β strands (Figure 6, light blue) interconnected by a turn that define an antiparallel β sheet inserted between the β strands depicted in pink and purple (Figure 6).

This comparative study highlights structural features that enable the binding of maltooligosaccharides to do-

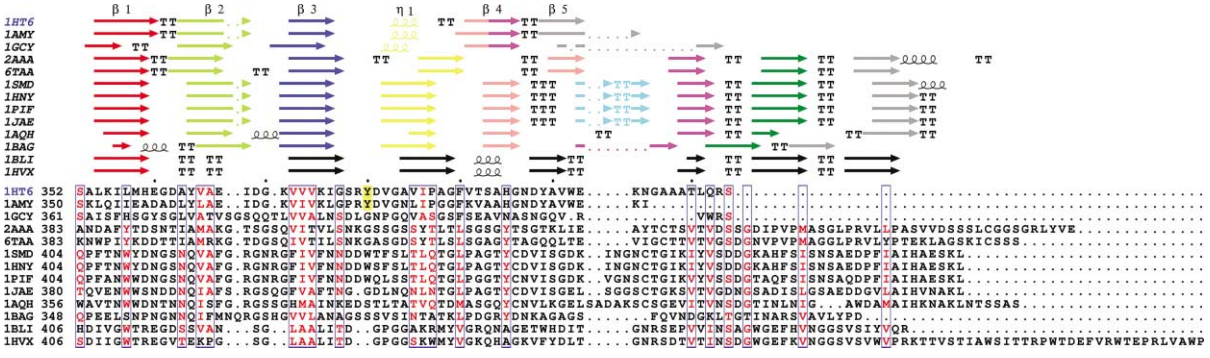

Figure 6. Primary and Secondary Structure Alignment of 12 α-Amylase C Domains from Different Species with a Maltotetraose-Forming Amylase

Each sequence is labeled by the Protein Data Bank entry code from which it has been extracted. Secondary structures are presented above the alignment and colored as a function of their spatial superimposability: structures superimposed or located in close vicinity are shown in the same color. β strands, arrows; α helices, helices; turn, T. Labels β1–β5 and η1 (η being helices with less than five residues) are attributed to AMY1 (1HT6). Gaps inserted in the sequence alignment are indicated by dots. Tyr380 in AMY1 numbering and its counterpart in AMY2 are highlighted in yellow, and blue boxes contouring red letters indicate most-homologous residues (or regions) in the sequence alignment.

Figure 7. Domain C from Different Amylases Superimposed on AMY1

AMY1 is presented in the color code from the sequence alignment in Figure 6, with the Tyr380 side chain highlighted in orange. From top to bottom are shown 1HSA, 1AQH, and 1GCY, all in cyan, with the β strand blocking the access to the sugar tongs site in AMY1 in dark green (see Figure 6).

main C in AMY1. Thus, in AMY1, the pair of sugar tongs with Tyr380 situated at the top of the domain is located between β3 and β4 and immediately precedes the small helix η1 in a region without particular secondary structure. The basis of the pair of sugar tongs is constituted by the part of the C domain that comprises the motif β4/turn/β5 forming an antiparallel β sheet. The loop containing Tyr380 is perpendicular to this antiparallel β sheet, and, together, they define a small cavity where sugars can bind and wind around Tyr380 (Figure 5). Residues 386–390 connecting η1 and β4 form a barrier that forces the maltooligosaccharide to adopt the curvature seen in Figure 5, and Tyr380 undergoes a significant positional shift upon sugar binding.

In conclusion, the presence of Tyr380 in a flexible region seems mandatory, but not sufficient, for creating a sugar binding site in domain C in AMY1. In addition to the flexible loop (Ser378–Pro387), an antiparallel β sheet motif (β4 and β5) is required. It appears that β4 is highly specific to AMY1 and AMY2, although its N- and C-terminal segments can be structurally aligned with two distinct β strands in certain other α-amylases (Figure 6). Furthermore, a β strand (Figure 6, dark green), inserted in α-amylases different from AMY1 and AMY2 and preceding the terminal β strand, β5, in AMY1 (Figure 6, gray), prevents formation of a binding site equivalent to the pair of sugar tongs in AMY1. Indeed, this β strand and, to a minor extent, the preceding one (Figure 6, purple) shortcut the domain C binding site in AMY1 and sterically hinder access to the sugar tongs (Figure 7).

Finally, we have compared domain C of AMY1 with the corresponding domain of the maltotetraose-forming amylase from *Pseudomonas stutzeri* (Mezaki et al., 2001). Interestingly, though this latter is an exo-acting α-amylase, its domain C is very similar in terms of tertiary structure to that of AMY1 (rmsd of 1.05 Å). As concerns their size, domains C of AMY1 and of the maltotetraose-forming amylase have 61 and 56 amino acid residues, respectively, and their five β strands are nearly perfectly superimposed. No β strand obstructs a hypothetical sugar tongs binding site, as seen in most of the enzymes compared in this study. However, in the three-dimensional structure of the maltotetraose-forming amylase, no tyrosine or other hydrophobic residue was found at a location comparable to $Tyr380_{AMY1}$. Moreover, the side chain of Arg414 in this enzyme seems to prevent the formation of a sugar tongs-like binding site by blocking the accessibility and preventing the binding of a polysaccharide chain.

So far, AMY1 appears to be unique among α-amylases in its capacity of binding maltooligodextrines and, probably, polysaccharide substrates in domain C. Though domain C of AMY2 is highly similar, this binding site does not exist in AMY2. $Pro376_{AMY2}$ ($Ser378_{AMY1}$) possibly impedes the loop mobility necessary for accommodation of the sugar, and mutational analysis of structural requirements for sugar binding in the Tyr380 region has been initiated. The structure of the AMY1/thio-DP4 complex thus unveils a possible biological role of domain C, characteristic of the AMY1 type of plant α-amylases

Table 1. Data Collection and Refinement Statistics for Native AMY1 and AMY1/Thio-DP4

	Native AMY1	AMY1/Thio-DP4
Wavelength (Å)	0.9761	1.5418
Temperature (K)	100	100
Cell dimensions (Å)	a = 88.36	a = 93.4
	b = 72.82	b = 72.1
	c = 61.74	c = 60.9
Space group	$P2_12_12$	$P2_12_12$
Resolution range (Å)	41.6–1.5 (1.54–1.5)	46.6–2.0 (2.11–2.0)
Completeness (%)	98.7 (97.3)	96.7 (96.7)
Total number of reflections	271,695	83,778
Number of unique reflections	63,366	27,556
Redundancy	4.3 (3.5)	3.0 (3.0)
R_{sym} (%)[a]	4.5 (11.9)	12.4 (47.6)
Overall I/σ(I)	13.3 (6.2)	5.7 (1.6)
R_{factor} (%)[b]	13.6 (14.4)	17.1 (20.8)
R_{free} (%)[c]	16.3 (17.3)	21.9 (26.0)
Rms deviation from ideal geometry		
Bond lengths (Å)	0.017	0.012
Bond angles (°)	1.70	1.34

Outermost shell values are indicated in parentheses.

[a] $R_{sym} = \Sigma_{hkl}\Sigma_i|I(hkl)_i - <I(hkl)>|/\Sigma_{hkl}\Sigma_i I(hkl)$.

[b] $R = \Sigma_h||F_{obs}(h)| - k|F_{calc}(h)||/\Sigma_h|F_{obs}(h)|$, where k is a scaling factor.

[c] $R_{free} = \Sigma_h||F_{obs}(h)| - k|F_{calc}(h)||/\Sigma_h|F_{obs}(h)|$, where k is a scaling factor calculated from a test set constituted by 10% of the total number of reflections randomly selected.

and, apparently, consistent with the higher affinity for starch granules (Rodenburg et al., 1994). This new noncatalytic site might, together with the previously identified surface binding site in domain A, participate in disentanglement of α-glucan chains in starch, in agreement with the more efficient attack of AMY1 on starch granules. We propose that both surface sites act to select and orient the substrate chains for hydrolysis at the active site by securing proper positioning of the enzyme and the compact substrate.

α-Amylases from cereals are involved in mobilization of seed storage stocks. They are essential in the production of beer and other beverages and in the baking industry. Designer enzymes having improved specificity, activity, or synergy with enzyme partners in the agro-alimentary and biotechnological domains provide important prospects. Engineering of this domain C surface binding site into AMY2 or other plant or even microbial α-amylases would most probably enhance their catalytic power on raw starch and related substrates.

The fact that only plant α-amylases and, more particularly, the AMY1 type display this property makes domain C of AMY1 a good candidate for use in chimeric enzymes. Combining the catalytic properties of, for example, psychrophilic α-amylases, which hydrolyze polysaccharides at low temperature, and the capacity of enhanced starch binding of AMY1 could result in a chimeric α-amylase with high efficiency on starch at low temperature.

Experimental Procedures

Crystallization, Data Collection, Processing, and Structure Refinement

AMY1Δ9 (herein referred to as AMY1) was produced by heterologous expression in *Pichia pastoris* and crystallized as described earlier (Robert et al., 2002a). The AMY1/thio-DP4 complex was obtained by soaking a crystal in 20% polyethylene glycol 8000 containing 10 mM thio-DP4 for 24 hr.

Diffraction data for AMY1 was collected as described elsewhere (Robert et al., 2002a). Data for the AMY1/thio-DP4 complex were collected in-house on a MAR345 image plate detector, with CuK_α radiation generated from a Nonius rotating anode operated at 4.4 kW and coupled to Osmic mirrors. The crystal was cryoprotected as native AMY1 (Robert et al., 2002a) and maintained at 100 K under a nitrogen stream during the entire data collection. Integration of the diffracted intensities was performed with the program DENZO (Otwinoswki and Minor, 1997), and scaling was performed with the program SCALA from the CCP4 software suite (CCP4, 1994). Table 1 gives a summary of the data collection statistics.

Though the soaking experiment did not modify the space group, an important increase in the *a* axis of 5 Å occurred, whereas only small variations were present along the *b* and *c* axes. The synthesis of thio-DP4 was achieved by an extension of the method already published (Blanc-Muesser et al., 1992) and is fully described elsewhere (Ratajczak et al., 2003).

The three-dimensional structure of native AMY1 was solved by the molecular replacement method with AMoRe software as implemented in the CCP4 suite and described previously (Robert et al., 2002a). As concerns the complex AMY1/thio-DP4, the refined 1.5 Å resolution structure of native AMY1 was used as a search model in AMoRe, and a unique solution with a correlation coefficient of 75.5% and an R factor of 30.4% was obtained, with diffraction data in the resolution range of 15–4 Å. Model building and/or manual refitting of the amino acid residues and insertion of calcium ions, water, ligands, and sugar molecules were performed with TURBO-FRODO (Roussel and Cambillau, 1989). The refinement of the model was done with the simulated annealing protocol from CNS (Brünger et al., 1998), alternated with manual rebuilding. In order to avoid overrefinement, the crystallographic R factor and R_{free} (Brünger, 1992) were monitored. The latter was calculated from a test set constituted by 10% (6406) of the reflections randomly selected from the native AMY1 data and 2744 reflections for the complex.

Water molecules were inserted manually if electron densities of at least 3 σ in the difference $F_o - F_c$ map and 1 σ in the $2F_o - F_c$ map were located and omitted if the B factor was superior to 60 $Å^2$ after refinement. The mean B factors for all solvent molecules are 26.5 $Å^2$ (native AMY1) and 22.1 $Å^2$ (AMY1/thio-DP4), and, for consistency, water molecules present at positions similar to those in the AMY2 structure have the same numbering. For amino acid residues displaying double conformations, the occupancy was refined. Unexplained electron densities in the $2F_o - F_c$ map contoured at 1 σ and

in the $F_o - F_c$ map contoured at 3 σ were examined and could be clearly described as ordered ethylene glycol molecules.

The final R factor for the native structure was 13.6%, with an R_{free} of 16.3% for all data within the 41.6–1.5 Å resolution range. The R factor and Rfree for the complex were 17.1% and 21.9%, respectively, for all data within the 46.6–2.0 Å resolution range. Table 1 gives a summary of the refinement statistics. The quality of both three-dimensional structures, in terms of geometry and coordinate errors, has been examined with the program WHATCHECK (Hooft et al., 1996).

Alignment and Figure Rendering

For the comparative studies of C domains, only experimental native structures have been considered. A search in the Protein Data Bank (Berman et al., 2000) resulted in the selection of 13 structures: barley α-amylase 1—AMY1 reported in this study (Protein Data Bank entry code 1HT6), barley α-amylase 2—AMY2 (1AMY) (Kadziola et al., 1994), maltotetraose forming amylase (1GCY) (Mezaki et al., 2001), α-amylases from *A. niger* (2AAA) (Boel et al., 1990), *A. oryzae*—TAKA (6TAA) (Swift et al., 1991), human salivary (1SMD) (Ramasubbu et al., 1996), human pancreas (1HNY) (Brayer et al., 1995), porcine pancreas—PPA (1PIF) (Machius et al., 1996), *T. molitor* (1JAE) (Strobl et al., 1998), a psychrophilic α-amylase from *Ps. haloplanctis* (1AQH) (Aghajari et al., 1998a), *B. subtilis* (1BAG) (Fujimoto et al., 1998), *B. licheniformis* (1BLI) (Machius et al., 1998), and *B. stearothermophilus* (1HVX) (Suvd et al., 2001). The sequences of these 13 amylases were derived from the Protein Data Bank coordinate files, and the parts corresponding to domain C were cut out and aligned with the program CLUSTALW (Thompson et al., 1994). Secondary structures were obtained from the atomic coordinate files with the same algorithm for each sequence (DSSP) (Kabsch and Sander, 1983) to obtain comparable results. In addition to the primary/secondary structure alignment, a tertiary structure alignment was performed with the aim of superimposing all 13 enzymes. The sequence alignment, which is grouped according to the species to emphasize sequence similarities, shows very weak overall sequence similarity. This primary structure alignment, including superimposition of secondary structure and domains of AMY1 and AMY2, was rendered with the program ESPript (Gouet et al., 1999). Comparative studies of the 13 amylase 3D structures were performed with TURBO-FRODO (Roussel and Cambillau, 1989), which, prior to this analysis, were structurally aligned with the DiCE structural alignment program (http://www-cryst.bioc.cam.ac.uk/COMPARER). Drawings were generated with the programs TURBO-FRODO (Roussel and Cambillau, 1989), GRASP (Nicholls et al., 1991), ViewerLite (Accelrys, San Diego), Molscript (Kraulis, 1991), Raster3D (Merritt and Bacon, 1997), and Ligplot (Wallace et al., 1995).

Acknowledgments

A. Gajhede is gratefully acknowledged for assistance with preparation of AMY1 and AMY1Δ9. M.T. Jensen, H. Mori, and K.S. Bak-Jensen are thanked for many stimulating discussions. M. Roth and J.-L. Ferrer from the FIP BM30A beamline at the ESRF synchrotron (Grenoble, France) are acknowledged for technical advice during data collection.

This work was supported by the European Union Framework III and IV programs to the projects NEWAMASE BIO3-3008 and AGADE (Alpha-Glucan Active Designer Enzymes; BIO4-980022). Support from Centre National de la Recherche Scientifique and travel support from Institut Français, Copenhagen, are also gratefully acknowledged.

Received: March 13, 2003
Revised: May 26, 2003
Accepted: May 28, 2003
Published: August 5, 2003

References

Abe, J., Sidenius, U., and Svensson, B. (1993). Arginine is essential for the α-amylase inhibitory activity of the α-amylase/subtilisin inhibitor (BASI) from barley seeds. Biochem. J. *293*, 151–155.

Aghajari, N., Feller, G., Gerday, C., and Haser, R. (1998a). Crystal structures of the psychrophilic α-amylase from *Alteromonas haloplanctis* in its native form and complexed with an inhibitor. Protein Sci. *7*, 564–572.

Aghajari, N., Feller, G., Gerday, C., and Haser, R. (1998b). Structures of the psychrophilic *Alteromonas haloplanctis* α-amylase give insights into cold adaptation at a molecular level. Structure *6*, 1503–1516.

Ajandouz, E.H., Abe, J., Svensson, B., and Marchis-Mouren, G. (1992). Barley malt-α-amylase. Purification, action pattern, and subsite mapping of isozyme 1 and two members of the isozyme 2 subfamily using *p*-nitrophenylated maltooligosaccharide substrates. Biochim. Biophys. Acta *1159*, 193–202.

André, G., Buleon, A., Haser, R., and Tran, V. (1999). Amylose chain behavior in an interacting context. III. Complete occupancy of the AMY2 barley α-amylase cleft and comparison with biochemical data. Biopolymers *50*, 751–762.

Banner, D.W., Bloomer, A.C., Petsko, G.A., Phillips, D.C., Pogson, C.I., Wilson, I.A., Corran, P.H., Furth, A.J., Milman, J.D., Offord, R.E., et al. (1975). Structure of chicken muscle triose phosphate isomerase determined crystallographically at 2.5 Å resolution using amino acid sequence data. Nature *255*, 609–614.

Berman, H.M., Westbrook, J., Feng, Z., Gilliland, G., Bhat, T.N., Weissig, H., Shindyalov, I.N., and Bourne, P.E. (2000). The Protein Data Bank. Nucleic Acids Res. *28*, 235–242.

Bertoft, E., Andtfolk, C., and Kulp, S.E. (1984). Effect of pH, temperature, and calcium-ions on barley malt α-amylase isoenzymes. J. Inst. Brew. *90*, 298–302.

Blanc-Muesser, M., Vigne, L., Driguez, H., Lehmann, J., Steck, J., and Urbahns, K. (1992). Spacer-modified disaccharide and pseudotrisaccharide methyl glycosides that mimic maltotriose, as competitive inhibitors for pancreatic α-amylase: a demonstration of the "clustering effect". Carbohydr. Res. *224*, 59–71.

Boel, E., Brady, L., Brzozowski, A.M., Derewenda, Z., Dodson, G.G., Jensen, V.J., Petersen, S.B., Swift, H., Thim, L., and Woldike, H.F. (1990). Calcium binding in α-amylases: an X-ray diffraction study at 2.1 Å resolution of two enzymes from *Aspergillus*. Biochemistry *29*, 6244–6249.

Brayer, G.D., Luo, Y., and Withers, S.G. (1995). The structure of human pancreatic α-amylase at 1.8 Å resolution and comparisons with related enzymes. Protein Sci. *4*, 1730–1742.

Brünger, A.T. (1992). Free R value: a novel statistical quantity for assessing the accuracy of crystal structures. Nature *355*, 472–475.

Brünger, A.T., Adams, P.D., Clore, G.M., DeLano, W.L., Gros, P., Grosse-Kunstleve, R.W., Jiang, J.S., Kuszewski, J., Nilges, M., Pannu, N.S., et al. (1998). Crystallography and NMR system: a new software suite for macromolecular structure determination. Acta Crystallogr. D Biol. Crystallogr. *54*, 905–921.

Brzozowski, A.M., Lawson, D.M., Turkenburg, J.P., Bisgaard-Frantzen, H., Svendsen, A., Borchert, T.V., Dauter, Z., Wilson, K.S., and Davies, G.J. (2000). Structural analysis of a chimeric bacterial α-amylase. High-resolution analysis of native and ligand complexes. Biochemistry *39*, 9099–9107.

Bush, D.S., Sticher, L., van Huystee, R., Wagner, D., and Jones, R.L. (1989). The calcium requirement for stability and enzymatic activity of two isoforms of barley aleurone α-amylase. J. Biol. Chem. *264*, 19392–19398.

(CCP4) CCP4 Collaborative Computational Project, Number 4. (1994). The CCP4 suite: programs for protein crystallography. Acta Crystallogr. D Biol. Crystallogr. *50*, 760-763.

Fujimoto, Z., Takase, K., Doui, N., Momma, M., Matsumoto, T., and Mizuno, H. (1998). Crystal structure of a catalytic-site mutant α-amylase from *Bacillus subtilis* complexed with maltopentaose. J. Mol. Biol. *277*, 393–407.

Gibson, R.M., and Svensson, B. (1987). Identification of tryptophanyl residues involved in binding of carbohydrate ligands to barley α-amylase 2. Carlsberg Res. Commun. *52*, 373–379.

Gouet, P., Courcelle, E., Stuart, D.I., and Metoz, F. (1999). ESPript:

analysis of multiple sequence alignments in PostScript. Bioinformatics *15*, 305–308.

Hooft, R.W., Vriend, G., Sander, C., and Abola, E.E. (1996). Errors in protein structures. Nature *381*, 272.

Jones, R.L., and Jacobsen, J.V. (1991). Regulation of synthesis and transport of secreted proteins in cereal aleurone. Int. Rev. Cytol. *126*, 49–88.

Juge, N., Rodenburg, K.W., Guo, X.J., Chaix, J.C., and Svensson, B. (1995). Isozyme hybrids within the protruding third loop domain of the barley α-amylase $(\beta/\alpha)_8$-barrel. Implication for BASI sensitivity and substrate affinity. FEBS Lett. *363*, 299–303.

Kabsch, W., and Sander, C. (1983). Dictionary of protein secondary structure: pattern recognition of hydrogen-bonded and geometrical features. Biopolymers *22*, 2577–2637.

Kadziola, A., Abe, J., Svensson, B., and Haser, R. (1994). Crystal and molecular structure of barley α-amylase. J. Mol. Biol. *239*, 104–121.

Kadziola, A., Søgaard, M., Svensson, B., and Haser, R. (1998). Molecular structure of a barley α-amylase-inhibitor complex: implications for starch binding and catalysis. J. Mol. Biol. *278*, 205–217.

Kraulis, P.J. (1991). MOLSCRIPT: a program to produce both detailed and schematic plots of protein structures. J. Appl. Crystallogr. *24*, 946–950.

Larson, S.B., Greenwood, A., Cascio, D., Day, J., and McPherson, A. (1994). Refined molecular structure of pig pancreatic α-amylase at 2.1 Å resolution. J. Mol. Biol. *235*, 1560–1584.

Leah, R., and Mundy, J. (1989). The bifunctional α-amylase/subtilisin inhibitor of barley: nucleotide sequence and patterns of seed specific expression. Plant Mol. Biol. *12*, 673–682.

MacGregor, A.W., and Ballance, D.L. (1980). Hydrolysis of large and small starch granules from normal and waxy barley cultivars by α-amylases from barley malt. Cereal Chem. *57*, 397–402.

MacGregor, A.W., and Morgan, J.E. (1986). Hydrolysis of barley starch granules by α-amylases from barley malt. Cereal Foods World *31*, 688–693.

MacGregor, E.A., MacGregor, A.W., Macri, L.J., and Morgan, J.E. (1994). Models for the action of barley α-amylase isozymes on linear substrates. Carbohydr. Res. *257*, 249–268.

MacGregor, E.A., Janecek, S., and Svensson, B. (2001). Relationship of sequence and structure to specificity in the α-amylase family of enzymes. Biochim. Biophys. Acta *1546*, 1–20.

Machius, M., Vertesy, L., Huber, R., and Wiegand, G. (1996). Carbohydrate and protein-based inhibitors of porcine pancreatic α-amylase: structure analysis and comparison of their binding characteristics. J. Mol. Biol. *260*, 409–421.

Machius, M., Declerck, N., Huber, R., and Wiegand, G. (1998). Activation of *Bacillus licheniformis* α-amylase through a disorder → order transition of the substrate-binding site mediated by a calcium-sodium-calcium metal triad. Structure *6*, 281–292.

Matsui, I., and Svensson, B. (1997). Improved activity and modulated action pattern obtained by random mutagenesis at the fourth β-α loop involved in substrate binding to the catalytic $(\beta/\alpha)_8$-barrel domain of barley α-amylase 1. J. Biol. Chem. *272*, 22456–22463.

Merritt, E.A., and Bacon, D.J. (1997). Raster3D: photorealistic molecular graphics. Methods Enzymol. *277*, 505–524.

Mezaki, Y., Katsuya, Y., Kubota, M., and Matsuura, Y. (2001). Crystallization and structural analysis of intact maltotetraose-forming exo-amylase from *Pseudomonas stutzeri*. Biosci. Biotechnol. Biochem. *65*, 222–225.

Mori, H., Bak-Jensen, K.S., Gottschalk, T.E., Motawia, M.S., Damager, I., Moller, B.L., and Svensson, B. (2001). Modulation of activity and substrate binding modes by mutation of single and double subsites +1/+2 and −5/−6 of barley α-amylase 1. Eur. J. Biochem. *268*, 6545–6558.

Mori, H., Bak-Jensen, K.S., and Svensson, B. (2002). Barley α-amylase Met53 situated at the high-affinity subsite -2 belongs to a substrate binding motif in the β → α loop 2 of the catalytic $(\beta/\alpha)_8$-barrel and is critical for activity and substrate specificity. Eur. J. Biochem. *269*, 5377–5390.

Mundy, J., Svendsen, I., and Hejgaard, J. (1983). Barley α-amylase/subtilisin inhibitor. Isolation and characterization. Carlsberg Res. Commun. *48*, 81–90.

Nicholls, A., Sharp, K.A., and Honig, B. (1991). Protein folding and association: insights from the interfacial and thermodynamic properties of hydrocarbons. Proteins *11*, 281–296.

Otwinoswki, Z., and Minor, W. (1997). Processing of X-ray diffraction data collected in oscillation mode. Methods Enzymol. *26*, 307–326.

Qian, M., Haser, R., and Payan, F. (1995). Carbohydrate binding sites in a pancreatic α-amylase-substrate complex, derived from X-ray structure analysis at 2.1 Å resolution. Protein Sci. *4*, 747–755.

Quiocho, F.A. (1989). Protein-carbohydrate interactions: basic molecule features. Pure Appl. Chem. *61*, 1293–1306.

Ramasubbu, N., Paloth, V., Luo, Y.G., Brayer, G.D., and Levine, M.J. (1996). Structure of human salivary α-amylase at 1.6 Å resolution: implications for its role in the oral cavity. Acta Crystallogr. D Biol. Crystallogr. *52*, 435.

Ratajczak, F., Greffe, L., Cottaz, S., and Driguez, H. (2003). Convergent synthesis of 4-thiomaltooligosaccharides. Synlett *9*, 1253–1254.

Robert, X., Gottschalk, T.E., Haser, R., Svensson, B., and Aghajari, N. (2002a). Expression, purification and preliminary crystallographic studies of α-amylase isozyme 1 from barley seeds. Acta Crystallogr. D Biol. Crystallogr. *58*, 683–686.

Robert, X., Haser, R., Svensson, B., and Aghajari, N. (2002b). Comparison of crystal structures of barley α-amylase 1 and 2: implications for isozyme differences in stability and activity. Biologia (Bratisl.) Suppl. *11*, 59–70.

Rodenburg, K.W., Juge, N., Guo, X.J., Søgaard, M., Chaix, J.C., and Svensson, B. (1994). Domain B protruding at the third β strand of the α/β barrel in barley α-amylase confers distinct isozyme-specific properties. Eur. J. Biochem. *221*, 277–284.

Rodenburg, K.W., Vallée, F., Juge, N., Aghajari, N., Guo, X., Haser, R., and Svensson, B. (2000). Specific inhibition of barley α-amylase 2 by barley α-amylase/subtilisin inhibitor depends on charge interactions and can be conferred to isozyme 1 by mutation. Eur. J. Biochem. *267*, 1019–1029.

Rogers, J.C. (1985a). Conserved amino acid sequence domains in α-amylases from plants, mammals, and bacteria. Biochem. Biophys. Res. Commun. *128*, 470–476.

Rogers, J.C. (1985b). Two barley α-amylase gene families are regulated differently in aleurone cells. J. Biol. Chem. *260*, 3731–3738.

Rogers, J.C., and Milliman, C. (1983). Isolation and sequence analysis of a barley α-amylase cDNA clone. J. Biol. Chem. *258*, 8169–8174.

Roussel, A., and Cambillau, C. (1989). TURBO-FRODO (Mountain View, CA: Silicon Graphics).

Sidenius, U., Olsen, K., Svensson, B., and Christensen, U. (1995). Stopped-flow kinetic studies of the reaction of barley α-amylase/subtilisin inhibitor and the high pI barley α-amylase. FEBS Lett. *361*, 250–254.

Søgaard, M., and Svensson, B. (1990). Expression of cDNAs encoding barley α-amylase 1 and 2 in yeast and characterization of the secreted proteins. Gene *94*, 173–179.

Søgaard, M., Kadziola, A., Haser, R., and Svensson, B. (1993). Site-directed mutagenesis of histidine 93, aspartic acid 180, glutamic acid 205, histidine 290, and aspartic acid 291 at the active site and tryptophan 279 at the raw starch binding site in barley α-amylase 1. J. Biol. Chem. *268*, 22480–22484.

Strobl, S., Maskos, K., Betz, M., Wiegand, G., Huber, R., Gomis-Ruth, F.X., and Glockshuber, R. (1998). Crystal structure of yellow meal worm α-amylase at 1.64 Å resolution. J. Mol. Biol. *278*, 617–628.

Suvd, D., Fujimoto, Z., Takase, K., Matsumura, M., and Mizuno, H. (2001). Crystal structure of *Bacillus stearothermophilus* α-amylase: possible factors determining the thermostability. J. Biochem. (Tokyo) *129*, 461–468.

Svendsen, I., Hejgaard, J., and Mundy, J. (1986). Complete amino acid sequence of the α-amylase/subtilisin inhibitor from barley. Carlsberg Res. Commun. *51*, 43–50.

Svensson, B., Gibson, R.M., Haser, R., and Astier, J.P. (1987). Crystallization of barley malt α-amylases and preliminary X-ray diffraction studies of the high pI isozyme, α-amylase 2. J. Biol. Chem. *262*, 13682–13684.

Swift, H.J., Brady, L., Derewenda, Z.S., Dodson, E.J., Dodson, G.G., Turkenburg, J.P., and Wilkinson, A.J. (1991). Structure and molecular model refinement of *Aspergillus oryzae* (TAKA) α-amylase: an application of the simulated-annealing method. Acta Crystallogr. B *47*, 535–544.

Thompson, J.D., Higgins, D.G., and Gibson, T.J. (1994). CLUSTAL W: improving the sensitivity of progressive multiple sequence alignment through sequence weighting, position-specific gap penalties and weight matrix choice. Nucleic Acids Res. *22*, 4673–4680.

Truscheit, E., Frommer, W., Junge, B., Muller, L., Schmidt, D.D., and Wingender, W. (1981). Chemistry and biochemistry of microbial α-glucosidases inhibitors. Angew. Chem. Int. Ed. Engl. *20*, 744–761.

Vallée, F., Kadziola, A., Bourne, Y., Juy, M., Rodenburg, K.W., Svensson, B., and Haser, R. (1998). Barley α-amylase bound to its endogenous protein inhibitor BASI: crystal structure of the complex at 1.9 Å resolution. Structure *6*, 649–659.

Wallace, A.C., Laskowski, R.A., and Thornton, J.M. (1995). LIGPLOT: a program to generate schematic diagrams of protein-ligand interactions. Protein Eng. *8*, 127–134.